

Article

# Development of Novel Polymer Supported Nanocomposite GO/TiO<sub>2</sub> Films, Based on poly(L-lactic acid) for Photocatalytic Applications

Neda Malesic Eleftheriadou, Anna Ofrydopoulou, Myrsini Papageorgiou  and Dimitra Lambropoulou \*

Laboratory of Environmental Pollution Control, Department of Chemistry, Aristotle University of Thessaloniki, GR-541 24 Thessaloniki, Greece; nmalesice@chem.auth.gr (N.M.E.); anofr1991@gmail.com (A.O.); myrsinipapag@gmail.com (M.P.)

\* Correspondence: dlambro@chem.auth.gr; Tel.: +30-2310-997687

Received: 26 February 2020; Accepted: 20 March 2020; Published: 30 March 2020



**Abstract:** In the present study the development of novel polymer-supported nanocomposite graphene oxide (GO)–TiO<sub>2</sub> films, based on poly(L-lactic acid), one of the most exploited bioplastics worldwide, was explored for photocatalytic applications. The nanocomposites were synthesized and evaluated as photocatalysts for the removal of a mixture of nine antibiotics, consisting of two sulphonamides (sulfamethoxazole, sulfadiazine), three fluoroquinolones (levofloxacin, norfloxacin, moxifloxacin), one anti-TB agent (isoniazid), one nitroimidazole (metronidazole), one lincosamide (lincomycin) and one diaminopyrimidine (trimethoprim), which are commonly found in wastewaters. The films were synthesized using 1 wt% GO and different TiO<sub>2</sub> content (10, 25, and 50 wt%) and characterized using Fourier transform infrared spectroscopy (FTIR), wide-angle X-ray diffraction (WAXD), thermogravimetric analysis (TGA) and differential scanning calorimetry (DSC). Findings confirmed the successful immobilization of GO/TiO<sub>2</sub> in all cases. The PLLA–GO–TiO<sub>2</sub> 50 wt% composite film demonstrated higher photocatalytic efficiency and, thus, was further investigated demonstrating excellent photostability and reusability even after four cycles. Overall, PLLA–GO–TiO<sub>2</sub> 50 wt% nanocomposite demonstrated high efficiency in the photocatalytic degradation of the antibiotics in various matrices including pure water and wastewater.

**Keywords:** antibiotics; bioplastics; graphene oxide; nanocomposites; photocatalysis; poly (L-lactic acid); titanium dioxide

## 1. Introduction

The occurrence of contaminants of emerging concern (ECs) in wastewater has been highlighted globally due to the potential irreversible effects on human health and aquatic biota [1]. According to their presence in household products [2,3], they have been identified in wastewater influents [4] which has become a worldwide issue [5–7]. These compounds are characterized as “pseudo-persistent” and due to their water soluble residuals they are categorized as compounds of “emerging” concern [8–10].

Antibiotics are widely used [11–14] and usually present in urine and faeces of humans and animals since a small percentage is metabolized and the rest is excreted unaltered [2,15–18]. They are continuously detected in surface waters [4] and even in low concentrations they are considered a risk for human health and the ecological environment since their residues can promote the development of bacteria with antimicrobial resistance (AMR), thus evolving the ability to sidestep the activity of antibiotics towards them. The issue of antibiotic removal from wastewater treatment processes is present due to their inability to biodegrade completely [12,19], thus becoming secondary pollutants

that could be further detected in the receiving waters [13,19–21]. The problem can be minimized if actions are taken to ameliorate the effectiveness of wastewater treatment processes in removing antibiotics and control their release to aquatic ecosystems [21].

As mentioned above, difficulties of antibiotic removal from WWTP effluents still exists [4,22] and there is a necessity in developing new methods [23,24] as alternatives to the conventional treatment for decontaminating water containing non-biodegradable organic compounds [25]. Advanced oxidation processes (AOPs) have been developed and have been recognized lately as emerging technologies due to their effectiveness in degradation of organic compounds [8,26]. Among different AOPs, semiconductor photocatalytic technology represented by titanium dioxide ( $\text{TiO}_2$ ) is regarded a promising water and wastewater treatment method [26].  $\text{TiO}_2$  is a non-toxic, stable photocatalyst with high photocatalytic activity under UV irradiation, and it is considered as the most promising photocatalyst for the oxidation of organic pollutants [23,24,26–28]. However,  $\text{TiO}_2$  is characterized by low quantum efficiency, fast recombination of the photoexcited electron-hole pairs and wide band gap resulting in limited performance under visible light [29,30] with a tendency for aggregation and weak recycling ability [31]. To overcome some of these drawbacks, the combination of semiconductors with carbon-based materials such as graphene oxide (GO) has been reported. The GO demonstrates a beneficial role in photocatalysis since it improves the adsorbance of the contaminants and plays the role of an electron acceptor, thus hindering the electron-hole recombination. Additionally, GO can act as a photosensitizer extending the light adsorption of GO/ $\text{TiO}_2$  nanocomposites into the visible region [32].

Apart from the previously mentioned limitations, there are still some drawbacks that hinder the implementation of suspended powder  $\text{TiO}_2$  photocatalysts in large-scale units. Among them, post separation for the recovery of the very fine particles of the photocatalyst and the feasibility of reuse of the recovered catalyst are considered the most prominent challenges since they render the whole process unprofitable. To overcome this drawback, the immobilization of the  $\text{TiO}_2$  catalyst on different polymer-supporting materials has been recently proposed [33–35]. In the latter case, immobilization of  $\text{TiO}_2$  on a membrane or a film demonstrates the advantage of acting also as a barrier for contaminants and their degradation products, thus improving the efficiency of the process. Consequently, employing new catalysts with immobilized  $\text{TiO}_2$  nano-sized particles proved to be a promising alternative that might facilitate the application of photocatalysis in real treatments.

In this context, herein, poly(L-lactic acid) nanocomposite (PLLA) was proposed as a supportive polymer for the immobilization of GO- $\text{TiO}_2$  nanoparticles. PLLA is one of the most commercially available bioplastics which has received considerable attention due to its nontoxicity, biocompatibility, biodegradability, biorenewability and good processability [36,37]. PLLA found application in miscellaneous fields like food packaging, tissue engineering and drug delivery systems [36–38]. For example, Athanasoulia et al. (2018) incorporated  $\text{TiO}_2$  particles into PLLA polymers via extrusion melt blending in order to test bactericidal efficiency under UV-light and low crystallinity of the poly(L-lactic acid) matrix. Likewise, Buzarovska et al. improved their biomedical application, by using thermally-induced phase separation (TIPS), due to their efficient antibacterial properties and good characteristics of the polymer matrix [36]. Despite the number of studies conducted in PLLA-based polymer materials recognizing its high potential, few data are currently available for the use of PLLA and its incorporation in photocatalytic applications [39–43]. Very recently, an interesting review has been published by Kaseem et al. [43] describing the experimental approaches used to improve the compatibility of PLA/ $\text{TiO}_2$  composites. Most of the reviewed studies, however, focused on the antimicrobial properties of PLA/ $\text{TiO}_2$  materials, while a handful of them are dedicated on their photocatalytic performance by using organic dyes a model compound [39–42]. To the best of our knowledge, PLA/ $\text{TiO}_2$  materials have not been reported until now for the photocatalytic degradation of emerging contaminants, like antibiotic compounds.

Based on the above, to allow the easy recovery and possible reuse of the photocatalyst, novel floating, polymer-supported nanocomposite GO/ $\text{TiO}_2$  films, based on poly(L-lactic acid), were prepared and characterized. The efficiency of the new photocatalysts was evaluated in eliminating a mixture

of nine antibiotics in two types of water matrices (pure water and wastewater effluent). Previous studies usually focus on the degradation of individual compounds. However, synergistic effects and the complexity of cocktail effects underline the importance of their study as a mixture [44]. Kinetics and detoxification of the treated solution were investigated in order to give an integrated evaluation of the newly synthesized nanocomposite films. Finally, the durability of the synthesized PLLA–GO–TiO<sub>2</sub> 50 wt% composite film as photocatalyst was evaluated during multiple treatment cycles. Thus far, the use of PLLA–GO–TiO<sub>2</sub> for water wastewater treatment is still in its inception. To the best of our knowledge, such study has not been conducted before.

## 2. Materials and Methods

### 2.1. Materials and Reagents

PLLA used for the preparation of the film was purchased under the trade name Purasorb PL38 (Purac Biochem, Gorinchem, The Netherlands). Its inherent viscosity was 3.81 dL/g (M<sub>n</sub> = 700,000 Da) and the water content less than 0.5%. The GO was synthesized by using a modified Staudenmaier's approach [45]. Accordingly, 10 g of powdered graphite was added to an acid mixture (concentrated H<sub>2</sub>SO<sub>4</sub> and HNO<sub>3</sub>) in an ice-water bath for cooling. Subsequently, potassium chlorate powder was added carefully to the mixture in small portions while stirring and cooling. After 18 h the mixture was poured into distilled water and the oxidation product was finally washed with distilled water until pH 6 and left to dry at room temperature. Titanium dioxide P25 was used as received from Evonik (Darmstadt, Germany) (particle size 20–30 nm; crystal structure: ~80% anatase and 20% rutile; surface area: 56 m<sup>2</sup> g<sup>-1</sup>, zero point of charge ≈ 6.3–6.8). All used antibiotics (sulfamethoxazole, sulfadiazine, isoniazid, trimethoprim, norfloxacin, moxifloxacin, lincomycin, levofloxacin) were obtained from Sigma Aldrich (Taufkirchen, Germany) with high purity (>98%). LC-MS-grade methanol was purchased by Merck (Darmstadt, Germany) and formic acid LC-MS grade (98%) was supplied by Sigma-Aldrich (Taufkirchen, Germany). Ultrapure water that was used for experiments and chromatographic analysis was obtained from a Millipore Waters Milli-Q water purification system. The solutions of antibiotics used for the experiments were freshly prepared before treatment by spiking the target antibiotics (1 mg/L) in ultrapure water or wastewater effluent which was previously filtered using a 0.45 μm pore size filter.

### 2.2. Synthesis of Films

The preparation of the films was based on the phase inversion method by which PLLA was firstly dissolved in a mixture of Trifluoroacetic acid (TFA)/chloroform (CHCl<sub>3</sub>) 25/75 v/v to prepare a viscous solution (5 wt%) which was then carefully poured into a glass casting support using doctor blade in order to obtain the required film thickness (150 μm). Subsequently, solvent was evaporated at room temperature and the prepared films have been further dried under vacuum till constant weight. The nanocomposite films with the immobilized GO/TiO<sub>2</sub> particles were prepared by following the same procedure. In this case, after dissolution of PLLA, a mixture of dispersed GO and TiO<sub>2</sub> in a solvent was added under sonication for 5 min, and the procedure was continued, as described for neat PLLA. Three different films were finally prepared containing 1 wt% GO and 10, 25 and 50 wt% TiO<sub>2</sub>. All synthesized films have been vacuum dried at 60 °C for 24 h.

### 2.3. Characterization of PLLA–GO–TiO<sub>2</sub> Composite Films

#### 2.3.1. Wide Angle X-Ray Scattering

In order to investigate the crystallization of the PLLA and its nanocomposites with GO and TiO<sub>2</sub> a XRD diffractometer (Rigaku-Miniflex 600, Chalgrove, Oxford, UK) was employed using Cu Ka radiation and scanning temperature range from 5° to 80°.

### 2.3.2. Differential Scanning Calorimetry (DSC)

The thermal properties of PLLA and its nanocomposites with GO and TiO<sub>2</sub> were tested using a Perkin–Elmer, Pyris Diamond differential scanning calorimeter (DSC) calibrated with indium and zinc standards. All DSC measurements were carried out under N<sub>2</sub> of 10 mL/min. The samples of 5 ± 0.1 mg were sealed in aluminium pans, scanned from about 30 to 200 °C at a 20 °C/min heating rate, held for 5 min in order to erase any thermal history and then were supercooled to -65 °C with a cooling rate of 200 °C/min. Glass transition and melting temperatures were obtained through subsequent heating runs as previously described.

### 2.3.3. Thermogravimetric Analysis (TGA)

A SETARAM SETSYS TG-DTA 16/18 thermal analyser was employed for the determination of weight loss and thermal stability carried out in simultaneous TG/DTA (thermogravimetry/differential thermal analysis) measurements. The thermogram was obtained from ambient temperature up to 600 °C, with a heating rate of 20 °C min<sup>-1</sup> with a nitrogen flow rate (99.9%) at 30 cm<sup>3</sup> min<sup>-1</sup>.

### 2.3.4. Scanning Electron Microscopy (SEM)

In order to examine the morphology (structure and porosity) of the prepared films a SEM (JEOL JMS-840) was employed. Cross-sections were used covered with a carbon coating in order to provide good conductivity of the electron beam. Operating conditions were the following: accelerating voltage 20 kV, probe current 45 nA and counting time 60 s.

## 2.4. TiO<sub>2</sub> Photocatalytic Degradation Experiment

For the photocatalytic experiments under simulated solar irradiation an Atlas Suntest CPS+ solar simulator (Germany) was used. Illumination was performed with a xenon lamp (1.5 kW, 750 W m<sup>-2</sup>). All experiments were carried out in a 200 mL Pyrex glass reactor. The pH value of ultrapure water was approximately 6. The experiment was performed in two separate stages. In the first part, the appropriate amount of catalyst together with prepared solution of nine antibiotics (100 mL) was added in the glass reactor, and it was kept in the dark on a magnetic stirrer for 30 minutes in order to achieve adsorption equilibrium on the catalyst's surface. Then the lamp was turned on and during illumination samples were collected at different time points and filtered through 0.22 µm syringe nylon membrane filters. Finally, samples were injected in the LC-MS system for determination of the target compounds in positive (PI) ionization mode.

## 2.5. Analytical Procedures

### 2.5.1. Kinetic Studies—LC-MS Analysis

An LC-MS system by Shimadzu was employed for the quantitative analysis of antibiotics concentration equipped with an ESI ionization source operating in positive ionization mode (PI). The detector voltage was set at 1.65 kV and for the chromatographic separation an Athena C<sub>18</sub>, (4.6 mm × 250 mm × 5 mm particle size; CNW Technologies) column was used operating at a flow rate 0.4 mL min<sup>-1</sup> at 40 °C. Twenty microlitre (20 µL) samples were injected and the elution of the compounds was performed by a binary gradient consisting of water-0.1% formic acid (A) and methanol (B).

### 2.5.2. Mineralization Studies

A TOC (total organic carbon) analyser was used to evaluate the degree of mineralization of the irradiated samples (previously filtered through 0.22 µm syringe nylon membrane filters).

### 2.5.3. Toxicity Analysis

Daphnia toxicity test was conducted according to OECD 202 guideline for testing of chemicals. Briefly, after incubation of daphnia magna eggs for 72 to 80 h under illumination, hatching of the ephippia occurred. Forty millilitres (40 mL) of test solution was loaded into four wells (10 mL each well) on a multiwall and 20 daphnias, divided into four groups of five organisms each, were added at the sample test and at control samples containing standard freshwater. The multiwall was placed in the incubator at 20 °C in the dark and the immobilization was recorded at 24 and 48 hours and compared with control values.

## 3. Results and Discussion

### 3.1. PLLA–GO–TiO<sub>2</sub> Characterization

The incorporation of added GO and TiO<sub>2</sub> amounts into PLLA film was evaluated with thermogravimetric analysis (TGA). As can be seen from Figure 1a neat PLLA and its nanocomposites have almost similar behaviour during heating. There is a small mass loss till 170 °C (about 1.7%), due to water evaporation, while the main mass loss occurs between 350–450 °C with a maximum decomposition rate at 370 °C for neat PLLA and at 384 °C for nanocomposites (Figure 1b). Thus, it seems that the addition of GO and TiO<sub>2</sub> enhances the decomposition of PLLA, which is in good agreement with previous reported studies in PLA nanocomposites [46–48] as well as in PLLA/TiO<sub>2</sub> nanocomposites [36,37]. In neat PLLA almost all the material is decomposing since only a char (no degraded material) of about 0.3% was remaining at 600 °C. In nanocomposites this char is much higher, which is expected since both GO and TiO<sub>2</sub> are non-degraded materials at that temperatures, and its amount increases by increasing the GO–TiO<sub>2</sub> content. From mass loss curves it was calculated that in all nanocomposites the remaining char is very close to the initially added GO–TiO<sub>2</sub> amounts, which is a proof that these are incorporated successfully in films.

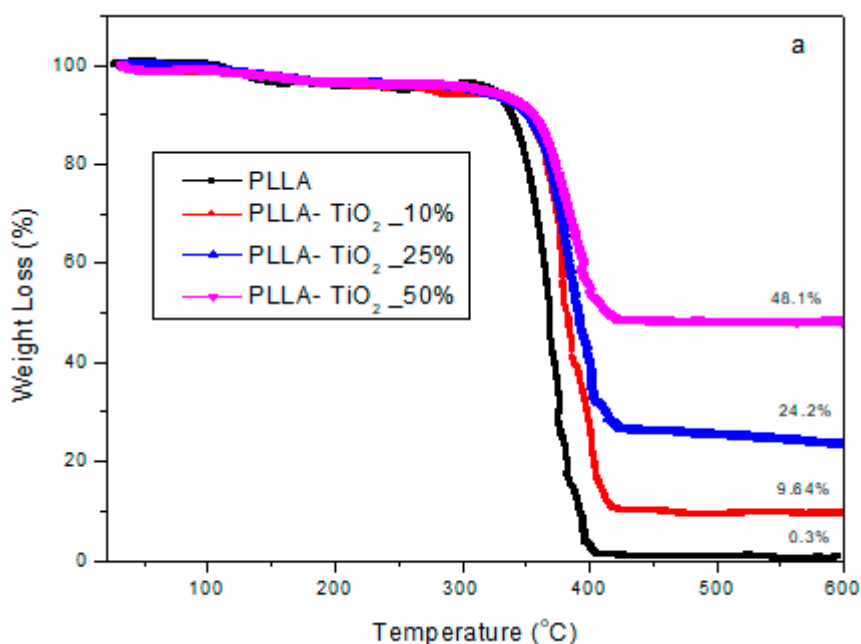


Figure 1. Cont.

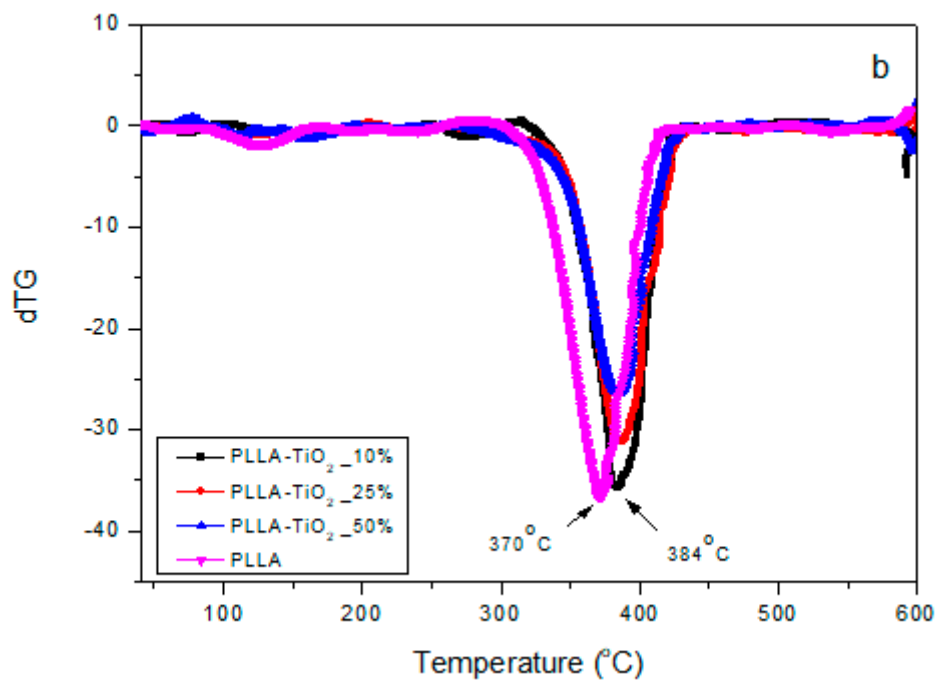
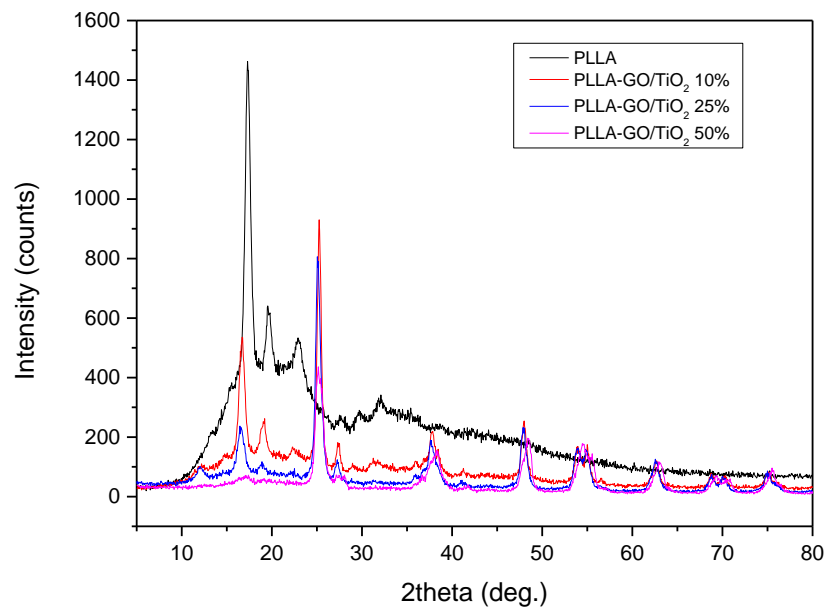


Figure 1. (a) Mass loss and (b) DTG curves of prepared PLLA GO-TiO<sub>2</sub> films.

The previous findings were also proved from XRD studies, since in all recorded patterns the characteristic peaks of TiO<sub>2</sub> can be found (Figure 2). TiO<sub>2</sub> NPs exhibited the anatase structure with peaks at 25.5° (101), 36.4° (103), 38° (004), 48.3° (200) and a double peak at 64.3–55.2° (105–211) while the small intensity peak at 27.6° (110) corresponds to a rutile structure [44]. Unfortunately, due to the small amount of GO in nanocomposites, any peak corresponded to them cannot be found on these patterns [47–50]. On the other hand, PLLA is a semicrystalline polymer with characteristic peaks at 17.31, 19.57 and 22.92°. These peaks can be found in all nanocomposites. However, it is evident that as the amount of GO-TiO<sub>2</sub> increases their intensity reduces. This was expected since the addition of inorganic nanoparticles in large amounts in a polymer, reduces the ability of macromolecules to be folded and, thus, its crystallisation behaviour. Similar findings were also mentioned by Athanasoulia et al. for PLLA/TiO<sub>2</sub> nanocomposites [37].

Some interactions between inorganic fillers and PLA matrix can be also responsible for this restriction to chain mobility. This was confirmed by FTIR spectroscopy (Figure 3). The main absorption peaks were observed at 3020 and 2943 cm<sup>-1</sup>, 1743 cm<sup>-1</sup> and 1177 cm<sup>-1</sup> due to CH stretching of methyl and methylene groups, stretching mode of the carboxyl ester groups and C-O groups, respectively. Additionally, some additional peaks were recorded at 1454 and 1381 cm<sup>-1</sup>, due to the asymmetric and symmetric deformation of CH<sub>3</sub> group and one broad and weak peak in the area 3500–3800 cm<sup>-1</sup> with a maximum at 3714 cm<sup>-1</sup> corresponding to the -OH end groups. TiO<sub>2</sub> nanoparticles have characteristic peaks at 807 cm<sup>-1</sup> corresponding to Ti-O-Ti groups and a broad peak of Ti-OH groups at 3200–3500 cm<sup>-1</sup>. On the other hand, GO exhibits lot of reactive groups like -OH, -COOH and epoxy groups. Absorption peaks hovering around 1630 cm<sup>-1</sup> was attributed to the C-O stretching vibrations of the COOH groups, while strong adsorptions at 1395 cm<sup>-1</sup> 1060 cm<sup>-1</sup> were assigned to the -C-OH deformations and C-O stretching vibrations, respectively. Moreover, exhibition of a peak at 1215 cm<sup>-1</sup> which was indexed to asymmetric stretching of C-O-C bridges in epoxy groups was observed [51]. However, due to its low amount in the prepared films (1 wt%) none of these peaks could be found in the recorded spectra. Comparing the spectra of prepared films with these of neat PLLA some characteristic shifts can be seen in the area of hydroxyl groups. In all nanocomposites the -OH absorbance is progressively shifted to lower wavenumbers by increasing the TiO<sub>2</sub> amount. This is an evidence that some interactions may be taking place between the -OH end groups of PLLA and

TiO<sub>2</sub>. On the contrary, the carbonyl group peak at 1743 cm<sup>-1</sup> remains stable, which is a proof that these peaks are not participated in any kind of interactions with TiO<sub>2</sub> groups.



**Figure 2.** XRD patterns of prepared films containing different GO–TiO<sub>2</sub> contents in comparison with neat PLLA and TiO<sub>2</sub> nanoparticles.

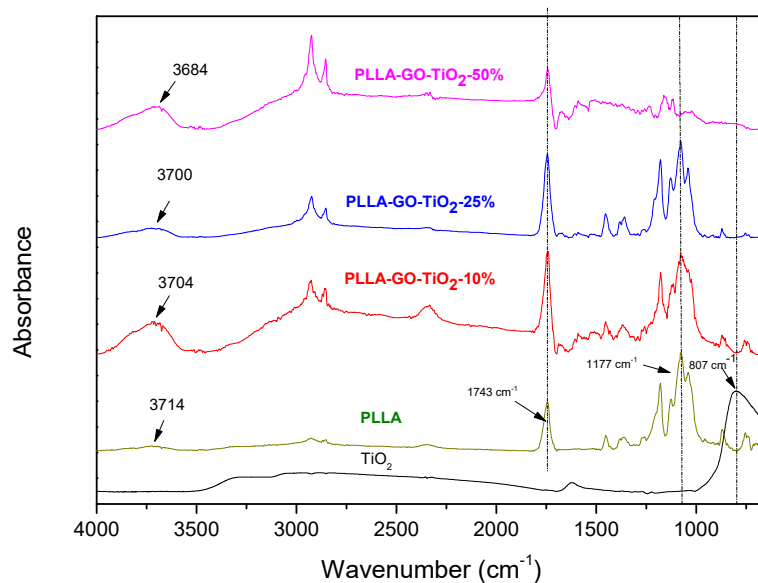


**Figure 3.** FTIR spectra of prepared films containing different GO–TiO<sub>2</sub> contents in comparison with neat PLLA and TiO<sub>2</sub> nanoparticles.

The addition of GO and mainly TiO<sub>2</sub>, which is in much higher amount compared with GO, nanoparticles affects also thermal properties of PLLA. As can be seen from Figure 4a PLLA is a semicrystalline material with melting point at 154.3 °C while the addition of nanoparticles causes a small reduction in melting point (about 1°C). This reduction seems not to be affected from the addition of TiO<sub>2</sub> amount. The same behaviour is observed in nanocomposites after quenching, in which the melting point is recorded at about 152–153 °C (Figure 4b).

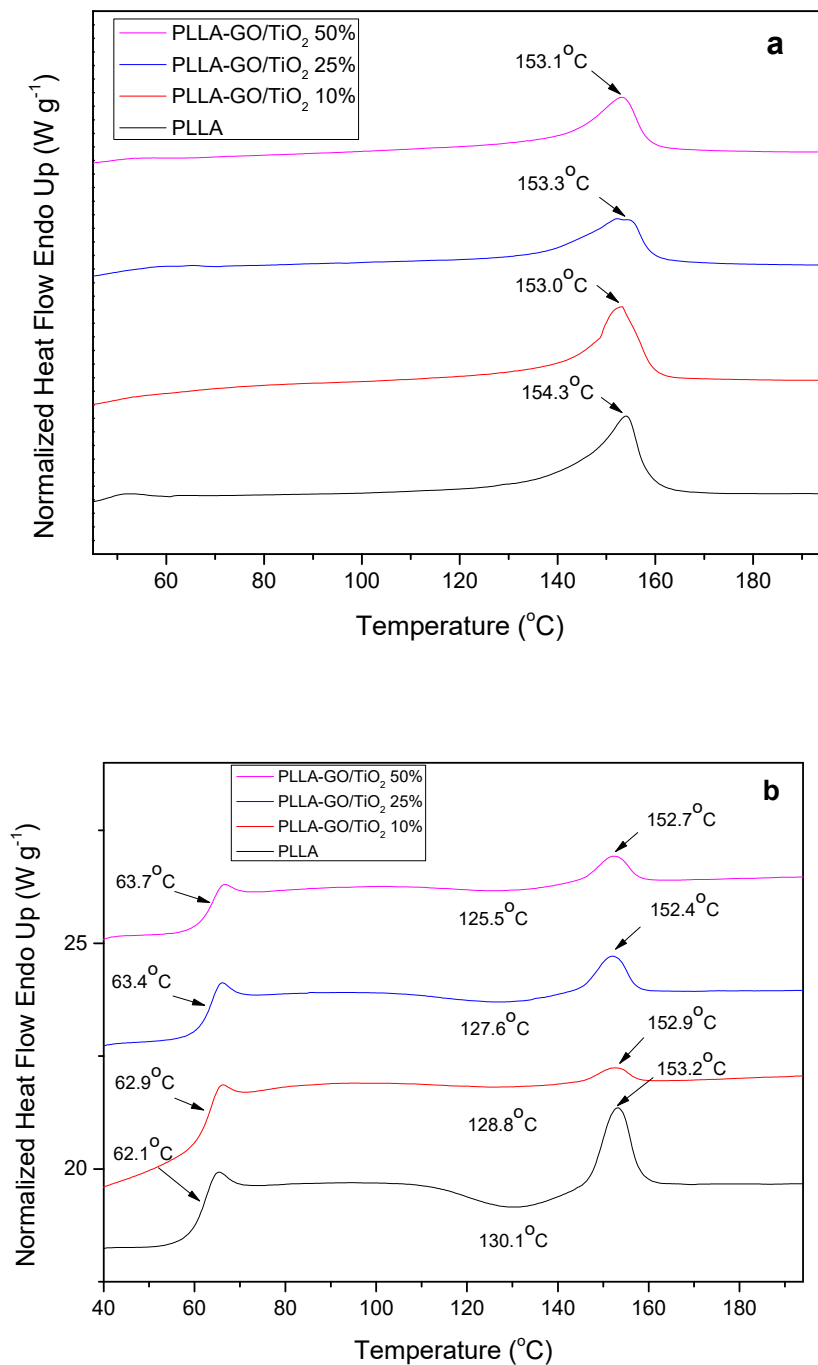


**Figure 4.** DSC thermograms of prepared nanocomposites containing different GO-TiO<sub>2</sub> contents in comparison with neat PLLA (a) as prepared samples and (b) melt quenched samples.

However, the glass transition temperature is progressively shifted to higher temperature, from 62.1 °C to 63.7 °C, as the amount of TiO<sub>2</sub> nanoparticles increases. This is due the formed interactions between PLLA and TiO<sub>2</sub>, as proved form FTIR spectroscopy, which hinders the segment mobility of macromolecules [52–55]. On the contrary, the addition of nanoparticles seems to enhance the crystallization of PLLA and, as can be seen by the cold crystallization temperature, which was recorded as an exothermal peak before the melting point of PLLA, it was progressively shifted to lower temperatures by increasing TiO<sub>2</sub> content. Similar crystallization behaviour was also mentioned for PLLA/SiO<sub>2</sub> nanocomposites [56].

### 3.2. PLLA–GO–TiO<sub>2</sub>-Based Photocatalysis

#### 3.2.1. Photocatalytic Degradation

The contribution of other processes like hydrolysis, adsorption or photolysis to the photocatalytic degradation process, were firstly examined. No hydrolytic effect was observed for any of the studied compounds. In order to examine the absorption of the target antibiotic compounds onto the newly synthesized catalyst, their mixture was left in the dark, in the presence of the composite film. After 30 min all the compounds were less than 1% adsorbed on the catalyst's surface except of moxifloxacin, norflaxacin and sulfadiazine, which exhibited a small adsorption reaching 15.8%, 11.6% and 6.1%, respectively. The photolytic effect was also examined by conducting experiments at the same initial concentration of the pharmaceuticals as in the photocatalytic run and in the absence of the catalyst. Results are depicted in Figure 5.

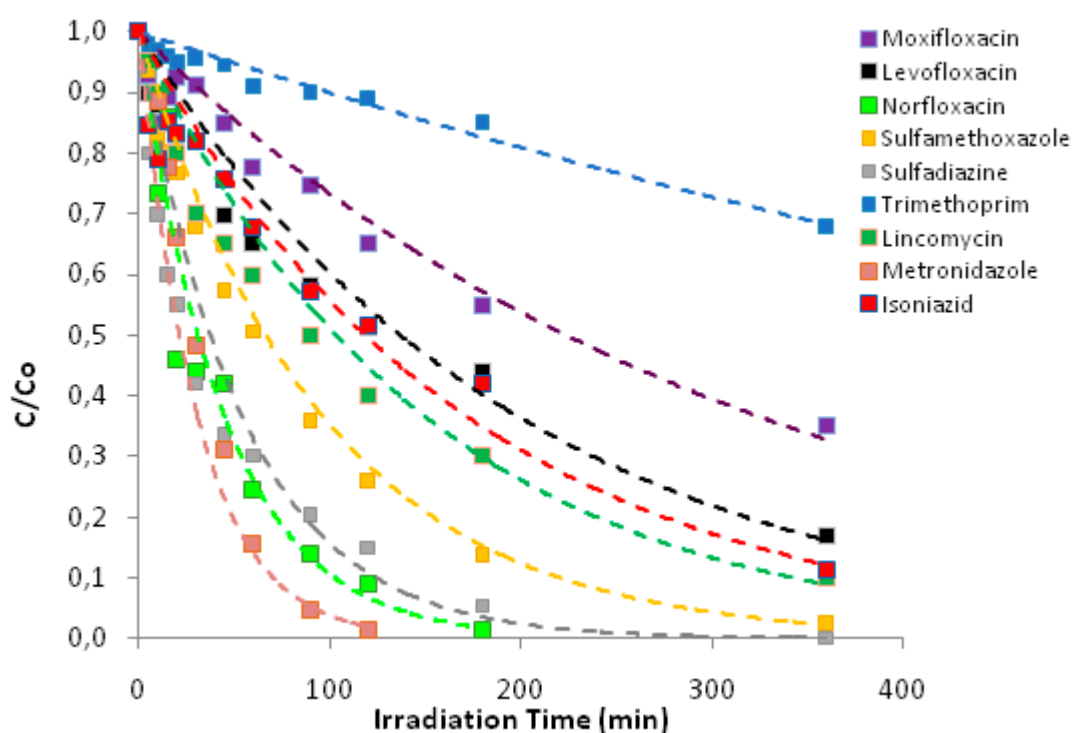
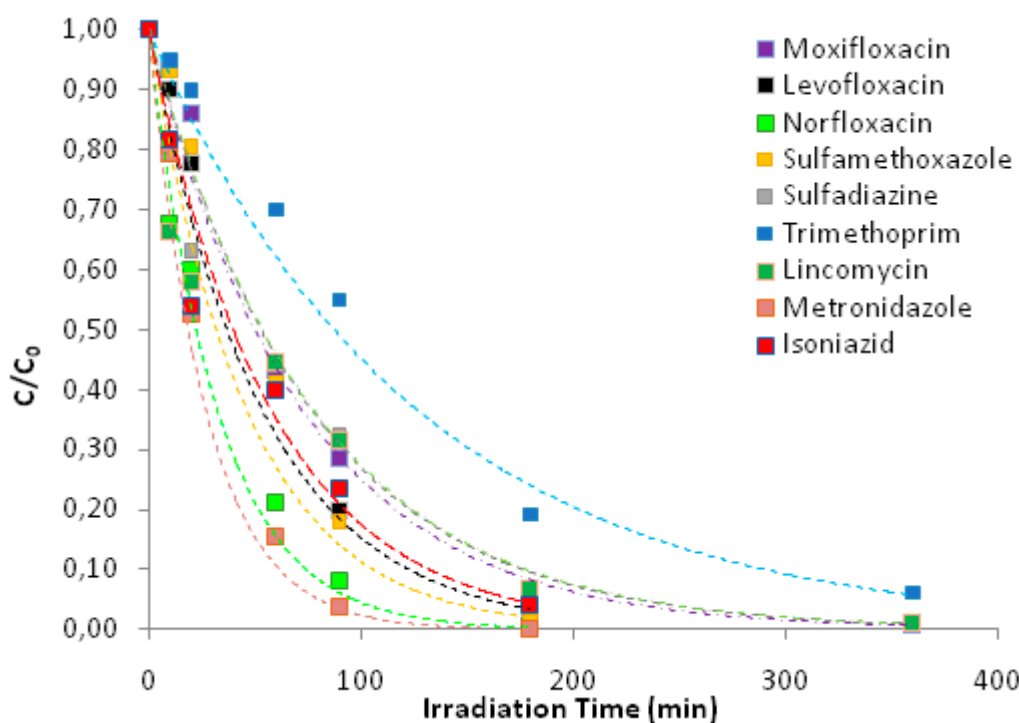


Figure 5. Photolytic degradation of antibiotics ( $C_{0\text{drug}} = 1 \text{ mg L}^{-1}$ ).

Obviously, as shown in Figure 5, all antibiotics are photolytically degraded since they exhibit adsorption at wavelengths above 290 nm, thus having an overlap with the emission spectrum of the lamp used. However, complete disappearance is only observed for metronidazole and norfloxacin after 120 and 180 min of illumination, respectively, while no other antibiotic is completely degraded after six hours of treatment. This is in accordance with previous studies [55] since norfloxacin belongs to the class of fluoroquinolones and it has been concluded that this class of antibiotics can undergo not only direct or indirect photolytic degradation but also a self-sensitised photo-oxidation via reactive oxygen species. The other two fluoroquinolones, moxifloxacin and levofloxacin, also undergo direct photolysis but at slower rates [55].

In Figure 6, the photocatalytic elimination of the mixture of antibiotics is depicted in the presence of the immobilized GO–TiO<sub>2</sub> on the composite film. All pharmaceutical compounds are almost completely eliminated within six hours of irradiation, thus indicating that even if photolysis is taking place its contribution to the overall photocatalytic process is smaller.



**Figure 6.** Photocatalytic elimination of the antibiotic mixture with PLLA–GO–50 wt% TiO<sub>2</sub> composite films ( $C_{0(\text{drug})} = 1 \text{ mgL}^{-1}$ , PLLA–GO–50 wt% TiO<sub>2</sub> = 1 gL<sup>-1</sup>, I = 750 Wm<sup>2</sup>).

More specifically, most of the compounds appear to be quite susceptible to photocatalysis since they are more than 90% degraded within 180 min of treatment while moxifloxacin, trimethoprim and lincomycin require more prolonged treatment.

According to the literature, the photocatalytic degradation follows the first order kinetic law expressed as in Equations (1) and the non-linear fit was applied to all photocatalytic degradation data [55]:

$$C = C_0 e^{-kt} \tag{1}$$

where  $k$  (min<sup>-1</sup>) is the apparent first order rate constant. In Table 1 all kinetic parameters, including the rate constants, the half-lives (min) calculated from Equation (2) and the regression coefficients  $R^2$  are presented:

$$t_{1/2} = \ln(2)/k \tag{2}$$

**Table 1.** Kinetic data during photolysis and photocatalysis of antibiotic mixture ( $C_{0(\text{drug})} = 1 \text{ mgL}^{-1}$ , PLLA–GO–50 wt% TiO<sub>2</sub> = 1 gL<sup>-1</sup>, I = 750 Wm<sup>2</sup>).

Categories	Antibiotics	Photocatalysis			Photolysis		
		k	t <sub>1/2</sub>	R <sup>2</sup>	k	t <sub>1/2</sub>	R <sup>2</sup>
Fluoroquinolones	moxifloxacin	0.014	49.5	0.98	0.003	231.0	0.96
	levofloxacin	0.019	36.5	0.99	0.005	138.6	0.97
	norfloxacin	0.031	22.4	0.99	0.020	34.7	0.98
Sulfonamides	sulfamethoxazole	0.022	31.5	0.97	0.010	69.3	0.99
	sulfadiazine	0.015	46.2	0.97	0.014	49.5	0.98
Diaminopyrimidines	trimethoprim	0.008	86.6	0.99	0.001	69.1	0.96
Lincosamides	lincomycin	0.013	53.3	0.98	0.007	99.0	0.98
Imidazoles	metronidazole	0.037	18.7	0.99	0.033	21.0	0.99
Hydrazide derivatives	isoniazid	0.017	40.8	0.98	0.006	11.5	0.97

Photolytic kinetic data were also calculated and included in Table 1 for comparison.

### 3.2.2. Effect of TiO<sub>2</sub> Content on PLLA Film

In order to investigate the effect of the TiO<sub>2</sub> loading on the photocatalytic degradation kinetics of the studied mixture, three different PLLA–GO–TiO<sub>2</sub> composite films were tested containing 10%, 25% and 50 wt% TiO<sub>2</sub>. In Table 2 all kinetic parameters (rate constants  $k$  (min<sup>-1</sup>), half-lives  $t_{1/2}$  (min) and regression coefficients, ( $R^2$ )) are presented.

**Table 2.** Effect of TiO<sub>2</sub> loading on kinetic parameters during the photocatalytic degradation of antibiotic mixture ( $C_{0(\text{drug})} = 1 \text{ mgL}^{-1}$ , PLLA–GO–TiO<sub>2</sub> =  $1 \text{ gL}^{-1}$ ,  $I = 750 \text{ Wm}^2$ ).

Antibiotics Fluoro-Quinolones	PLLA–10% wt TiO <sub>2</sub>			PLLA–25% wt TiO <sub>2</sub>			PLLA–50 wt% TiO <sub>2</sub>		
	k	$t_{1/2}$	$R^2$	k	$t_{1/2}$	$R^2$	k	$t_{1/2}$	$R^2$
moxifloxacin	0.013	53.3	0.97	0.014	49.5	0.98	0.014	49.5	0.98
levofloxacin	0.009	77.0	0.98	0.014	49.5	0.98	0.019	36.5	0.99
norfloxacin	0.020	34.7	0.97	0.023	30.1	0.96	0.031	22.4	0.99
Sulfonamides									
sulfamethoxazole	0.010	69.3	0.98	0.011	63.0	0.99	0.022	31.5	0.97
sulfadiazine	0.013	53.3	0.98	0.014	49.5	0.98	0.015	46.2	0.97
Diaminopyrimidines									
trimethoprim	0.003	231.0	0.99	0.005	138.6	0.98	0.008	86.6	0.99
Lincosamides									
lincomycin	0.008	86.6	0.97	0.012	57.8	0.98	0.013	53.3	0.98
Imidazoles									
metronidazole	0.032	21.7	0.96	0.033	21.0	0.99	0.037	18.7	0.99
Hydrazide derivatives									
isoniazid	0.009	77.0	0.98	0.016	43.3	0.97	0.017	40.8	0.98

Obviously, the composite film with the higher loading of TiO<sub>2</sub> is the most effective since higher reaction rates are achieved. The increase of the TiO<sub>2</sub> content sped up the photodegradation kinetics since more hydroxyl radicals are produced and more active sites are available for antibiotics degradation [24], [57]. Moreover, the use of a high TiO<sub>2</sub> dosage in an immobilized catalyst does not provoke the reduction of the reaction rate caused by light scattering and turbidity of the solution as it is usually observed in the suspended form of the catalyst [26]. Since the PLLA–GO–50%wt TiO<sub>2</sub> film exhibited the higher photocatalytic efficiency, it was selected to be further investigated.

### 3.2.3. Reusability Study of the PLLA–GO–50%wt TiO<sub>2</sub> Composite Film

In order to achieve the maximum efficiency of a catalyst, recycling and reuse are significant parameters to be investigated. Under this light, the photocatalytic activity of the PLLA–GO–50 wt% TiO<sub>2</sub> composite film was tested for four cycles. After each cycle the nanocomposite film was withdrawn from the reactor, washed with deionized water, dried and prepared for the next run.

In Table 3 all the calculated  $k$  values are depicted and in Figure 7a comparable degradation performance of one compound of the mixture, sulfamethoxazole, is illustrated for four consecutive cycles.

Obviously there is no observed reduction on the catalyst's efficiency for all antibiotics, indicating the stability of the composite film towards radiation and the •OH radicals which has been previously reported that may attack not only the organic pollutants but also the adjacent polymer chains [24,58]. Moreover, the observed capability of the catalyst to maintain its degradation efficiency after four cycles can be attributed to the strong attachment of TiO<sub>2</sub> particles on the polymer film as it is obvious in Figure 8. PLLA–GO–50 wt% TiO<sub>2</sub> composite films after their uses have been characterized by several techniques to detect any differences caused by the photocatalysis process. As it can be seen in Figure 8a, the initial PLLA–GO–50 wt% TiO<sub>2</sub> composite has smooth surface while after the first run of photocatalysis there are some micropores formed into its surface. These could be due to TiO<sub>2</sub> removal

or due to the partial decomposition of PLLA matrix due to photocatalysis. However, the surface and its porosity remain almost the same after the fourth run of photocatalysis and it seems to be unaffected from the additional runs.

**Table 3.** Effect of reusability of the PLLA–GO–50 wt% TiO<sub>2</sub> films on the kinetic data of the photocatalytic degradation of antibiotic mixture. C<sub>0</sub>(drug) = 1 mgL<sup>-1</sup>, PLLA–GO–TiO<sub>2</sub> = 1 gL<sup>-1</sup>, I = 750 Wm<sup>2</sup>.

Categories	Antibiotics	Cycles			
		k (min <sup>-1</sup> )			
		1 <sup>st</sup>	2 <sup>nd</sup>	3 <sup>rd</sup>	4 <sup>th</sup>
Fluoroquinolones	moxifloxacin	0.014	0.013	0.014	0.014
	levofloxacin	0.019	0.019	0.018	0.018
	norfloxacin	0.031	0.032	0.030	0.030
Sulfonamides	sulfamethoxazole	0.022	0.022	0.021	0.022
	sulfadiazine	0.015	0.014	0.015	0.016
Diaminopyrimidines	trimethoprim	0.008	0.009	0.007	0.008
Lincosamides	lincomycin	0.013	0.013	0.011	0.012
Imidazoles	metronidazole	0.037	0.035	0.037	0.033
Hydrazide derivatives	isoniazid	0.017	0.017	0.017	0.017

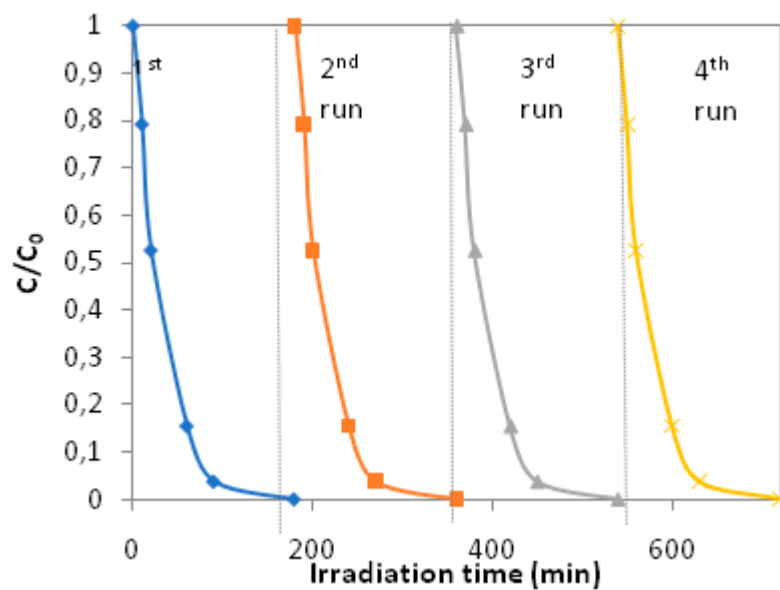


**Figure 7.** Recyclability test of PLLA–GO–50 wt% TiO<sub>2</sub> film on the photocatalytic degradation of sulfamethoxazole C<sub>0</sub>(drug) = 1 mg L<sup>-1</sup>, PLLA–GO–TiO<sub>2</sub> = 1 gL<sup>-1</sup>, I = 750 Wm<sup>2</sup>.

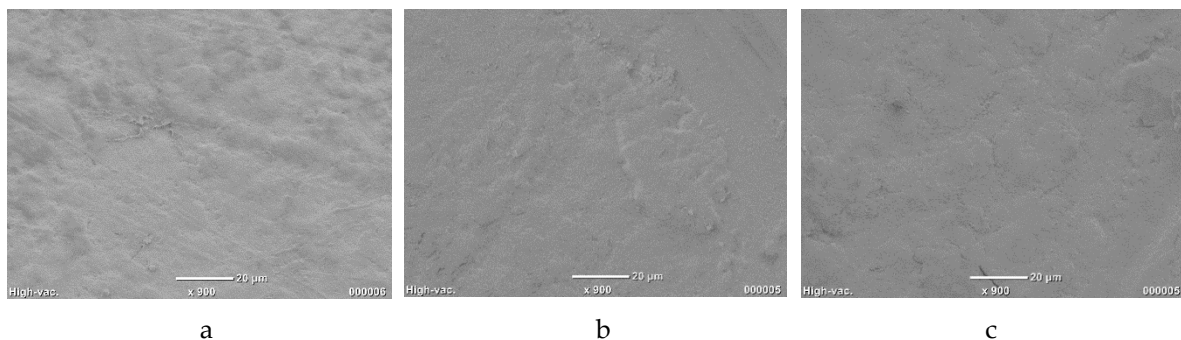


**Figure 8.** SEM micrographs of PLLA–GO/TiO<sub>2</sub> 50 wt%: (a) before photocatalysis, (b) after the second run and (c) after the fourth photocatalytic run.

Moreover, TGA analysis has been conducted in all PLLA-GO/TiO<sub>2</sub> 50 wt% films after several photocatalytic runs. As it can be seen in Figure 9, after the second run the mass loss is much higher, compared with the sample before photocatalysis, and the remaining char is about 45.8%. This is an indication that some small amount of TiO<sub>2</sub> (about 2.3%), which was probably located at the surface of prepared films, was removed during photocatalysis. This phenomenon was also repeated during 4<sup>th</sup> run where an additional 1.1% of TiO<sub>2</sub> was lost, since the remaining char is 44.7%. Similar results have been found in our previous studies in PET/TiO<sub>2</sub> films [24]. This removal can also explain the porosity of used films after several photocatalysis runs.

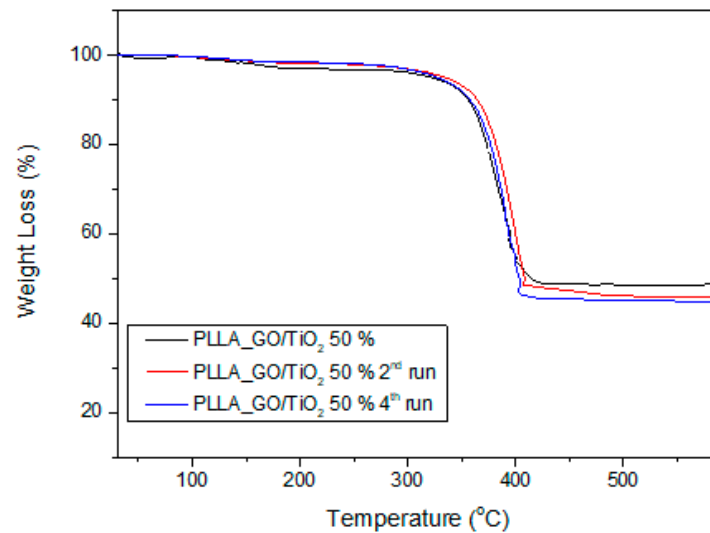


**Figure 9.** Mass loss of PLLA-GO/TiO<sub>2</sub> 50 wt% before photocatalysis, after the second run and after the fourth photocatalytic run.

Due to this small loss of TiO<sub>2</sub> during photocatalysis, very small differences have been also detected with DSC in PLLA-GO-50 wt% TiO<sub>2</sub> composites after several photocatalytic cycles (Figure 10). PLLA-50 wt% TiO<sub>2</sub> composite before its use has a melting point at about 153.1 °C, which remains almost the same after the second run and slight shifted to 152.1 °C after the fourth run.

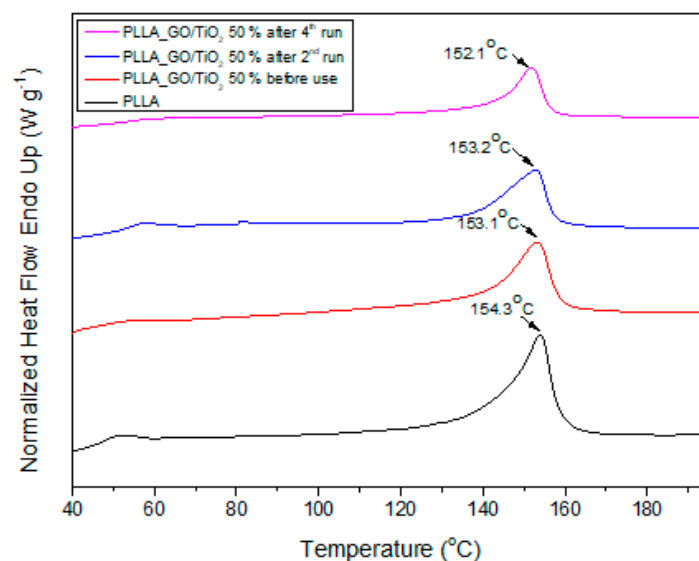


**Figure 10.** DSC thermograms of PLLA-GO/TiO<sub>2</sub> 50 wt% films before and after different photocatalytic runs.

### 3.2.4. Mineralization and Toxicity Evaluation

In order to investigate the degree of mineralization, TOC measurements were carried out during and at the end of the process. However, after 6 h of illumination less than 30% removal of the TOC was achieved indicating that recalcitrant intermediates are formed requiring more prolonged irradiation time for their elimination.

Since the formation of various transformation products throughout treatment may pose environmental risks [59] the evaluation of the changes in toxicity during treatment is indispensable. In the present study a *Daphnia magna* toxicity bioassay was applied to samples taken during the photocatalytic treatment and the immobilization of the organisms expressed as the % effect after 24 h and 48 h of exposure was determined. In Figure 11, the results from the bioassay are depicted.

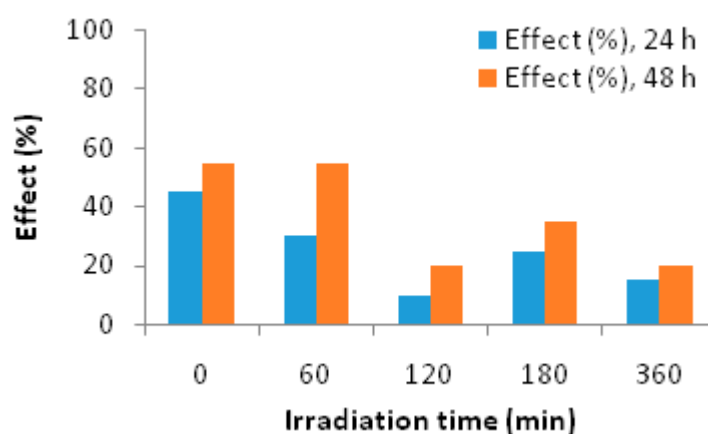


**Figure 11.** Changes in toxicity of the treated solution during photocatalytic treatment with PLLA–GO–50 wt% TiO<sub>2</sub>.  $C_{0(\text{drug})} = 1 \text{ mgL}^{-1}$ ,  $\text{PLLA-GO-TiO}_2 = 1 \text{ gL}^{-1}$ ,  $I = 750 \text{ Wm}^2$ .

Obviously, photocatalytic treatment of the target mixture leads to a reduction in toxicity in general. After 2 h of treatment toxicity appears a reduction from 55% effect to 20% (48h) since most of the compounds of the mixture are by this time more than 70% degraded. However, after three hours of illumination a slight increase is depicted despite the fact that most of the parent compounds are more than 90% degraded, thus indicating the formation of by-products that may pose a slight toxic effect on the tested organism. After six hours of treatment, a 20% effect is still observed probably due to the presence of recalcitrant intermediates as it has been also indicated by the slight reduction of TOC (less than 30%).

### 3.2.5. Evaluation of the Photocatalytic Efficiency of the PLLA–GO–50 wt% TiO<sub>2</sub> Composite Film on the Photodegradation of the Mixture of Antibiotics in a Wastewater Matrix

In order to examine the efficiency of the PLLA–GO–50 wt% TiO<sub>2</sub> composite film on the elimination of the target compounds being present in a wastewater matrix, experiments were conducted in a wastewater effluent obtained from an urban wastewater treatment plant. In Table 4, the physicochemical characteristics of the effluent are depicted.

In Figure 12, the photocatalytic degradation of the antibiotic compounds is presented. Obviously, the newly synthesized PLLA–GO–50 wt% TiO<sub>2</sub> composite film is effective enough to cause more than 90% degradation for most of the studied compounds.

In Table 5, all kinetic parameters are presented.

**Table 4.** Physicochemical characteristics of the wastewater effluent.

Physicochemical Parameters	Values
BOD (mgL <sup>-1</sup> )	11
COD (mgL <sup>-1</sup> )	59
SS (mgL <sup>-1</sup> )	8.4
N-NH <sub>3</sub> (mgL <sup>-1</sup> )	9.3
N-NO <sub>3</sub> (mgL <sup>-1</sup> )	1.5
P <sub>tot</sub> (mgL <sup>-1</sup> )	1.2
Bicarbonate (mgL <sup>-1</sup> )	380
Chloride (mg <sup>-1</sup> )	124
TOC (mgL <sup>-1</sup> )	14.3
pH	7.9

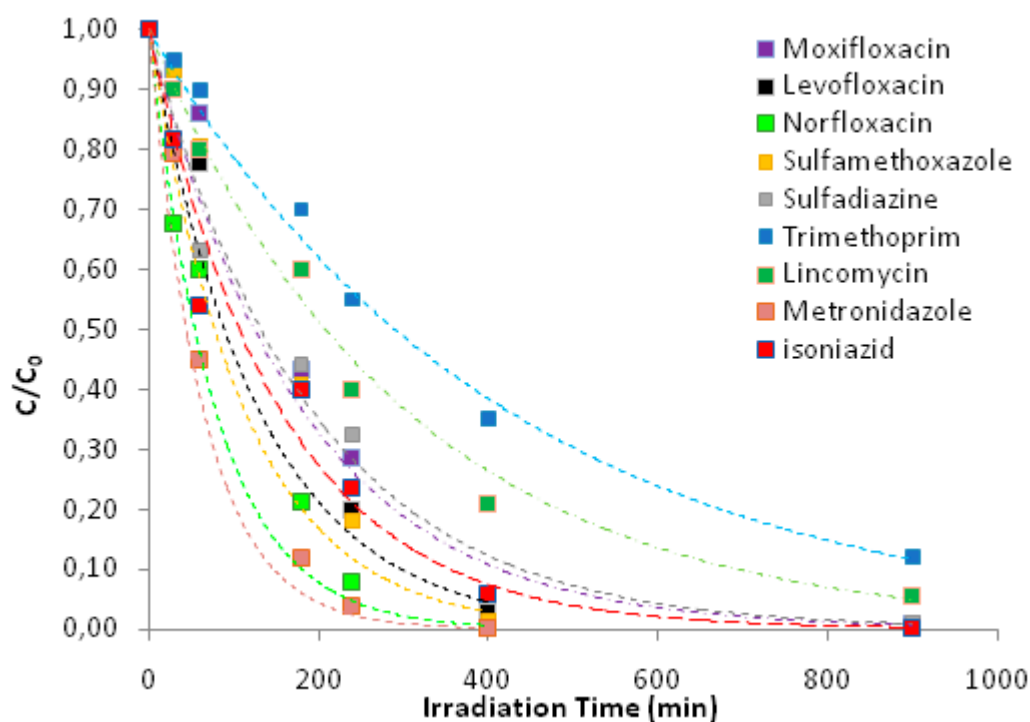


**Figure 12.** Photocatalytic degradation of the antibiotics mixture in the presence of PLLA-GO-50 wt% TiO<sub>2</sub> composite films in a wastewater effluent ( $C_{0(\text{drug})} = 1 \text{ mgL}^{-1}$ , PLLA-GO-50 wt% TiO<sub>2</sub> = 1 gL<sup>-1</sup>, I = 750 Wm<sup>2</sup>).

**Table 5.** Kinetic data of the photocatalytic degradation of antibiotic mixture in wastewater effluent. ( $C_{0(\text{drug})} = 1 \text{ mgL}^{-1}$ , PLLA-GO-50 wt% TiO<sub>2</sub> = 1 gL<sup>-1</sup>, I = 750 Wm<sup>2</sup>).

Categories	Antibiotics	Photocatalysis in Wastewater Effluent		
		k	t <sub>1/2</sub>	R <sup>2</sup>
Fluoroquinolones	moxifloxacin	0.0035	198.0	0.99
	levofloxacin	0.0048	145.9	0.98
	norfloxacin	0.0078	89.4	0.97
Sulfonamides	sulfamethoxazole	0.0055	126.0	0.96
	sulfadiazine	0.0038	184.8	0.97
Diaminopyrimidines	trimethoprim	0.002	346.6	0.99
Lincosamides	lincomycin	0.0033	213.3	0.99
Imidazoles	metronidazole	0.0093	74.9	0.99
Hydrazide derivatives	isoniazid	0.0043	163.1	0.98

Since the resulting correlation coefficients were  $R^2 > 0.96$ , the first-order simplified model can be also applied to adequately describe the degradation of the pharmaceutical compounds in a wastewater matrix. However, slower kinetics compared to ultrapure water are obtained due to this increase of the complexity of the matrix. Firstly, a significant role to the scavenging effect is played by the dissolved organic matter (~11 mg/L) which not only consumes the produced hydroxyl radicals since the latter lack of selectivity, but also competes with the target compounds for the active sites on the catalyst's surface, thus suppressing their degradation [31]. Moreover, inorganic ions that are present in wastewaters, like bicarbonates, chlorides or sulphates, can act as scavengers of hydroxyl radicals, thus prohibiting the photodegradation process of the pharmaceuticals [60].

#### 4. Conclusions

In the present study, novel polymer supported nanocomposite TiO<sub>2</sub> films, based on poly(L-lactic acid), a well-known bioplastic, have been synthesized and successfully applied for the photocatalytic degradation of a mixture of nine antibiotics which are commonly found at environmental samples. Characterization techniques such as FTIR, WAXD, TGA and DSC further confirmed their successful preparation. Among all prepared catalysts, PLLA–GO–50 wt% TiO<sub>2</sub> composite film showed better photocatalytic activity towards the treatment of the antibiotic mixture. The application was evaluated, comparing its efficiency during the treatment of ultrapure water and a wastewater effluent. Effective degradation of the target compounds was observed in both cases although slower kinetics was obtained for wastewater effluents due to the complexity of the matrix. After photocatalysis, the acute toxicity of antibiotics decreased suggesting that the formed TPs possessed similar or lower acute toxicity to aquatic organisms (*Daphnia magna*) and, therefore, applying the photocatalysis as a post-treatment technique would be beneficial for the elimination of antibiotics.

In conclusion, the reusability of the photocatalyst was assessed for four consecutive cycles. The findings revealed that the PLLA–GO–50 wt% TiO<sub>2</sub> composite film can be easily reused without losing efficiency and avoiding the need of additional post-treatment recovery. Thus, the proposed bioplastic materials provide new possibilities in the investigation of immobilized TiO<sub>2</sub> graphene composites on polymer films and promote their practical application in water and wastewater purification addressing various environmental issues.

**Author Contributions:** Conceptualization: N.M.E., A.O., M.P. and D.L.; methodology: N.M.E., A.O., M.P. and D.L.; software: N.M.E., A.O., M.P. and D.L.; validation: N.M.E., A.O., M.P. and D.L.; formal analysis: N.M.E., A.O., M.P. and D.L.; investigation: N.M.E., A.O., M.P. and D.L.; writing—original draft preparation: N.M.E., A.O., M.P. and D.L.; writing—review and editing: N.M.E., A.O., M.P. and D.L.; visualization: N.M.E., A.O., M.P. and D.L.; supervision: D.L.; All authors have read and agreed to the published version of the manuscript.

**Funding:** This research was funded in the context of the project “Antineoplastic and Antibiotic drugs in Aquatic Environment: Photocatalytic Degradation, Identification of Transformation Products, Toxicity Assessment and Antibiotic Resistance” (MIS: 5004700) under the call for proposals “Supporting researchers with emphasis on new researchers” (EDULLL 34). The project is co-financed by Greece and the European Union (European Social Fund-ESF) by the Operational Programme Human Resources Development, Education and Lifelong Learning 2014–2020.



**Acknowledgments:** The authors would like to specially acknowledge Dimitrios Bikiaris and Eleni Evgenidou from Dep. of Chemistry of Aristotle University of Thessaloniki for their helpful advice on various technical issues regarding the preparation of the materials and their photocatalytic application, respectively, as well as MSc. Evi Christodoulou and MSc. Nina Maria Ainali for their continuous encouragement during the implementation of this project.

**Conflicts of Interest:** The authors declare no conflict of interest.

## References

1. De Vidales, M.M.; Nieto-márquez, A.; Morcuende, D.; Atanes, E.; Blaya, F.; Soriano, E.; Fernández-martínez, F. 3D printed floating photocatalysts for wastewater treatment. *Catal. Today* **2019**, *328*, 157–163. [[CrossRef](#)]
2. Neghi, N.; Krishnan, N.R.; Kumar, M. Analysis of metronidazole removal and micro-toxicity in photolytic systems: Effects of persulfate dosage, anions and reactor operation-mode. *J. Environ. Chem. Eng.* **2018**, *6*, 754–761. [[CrossRef](#)]
3. Gonzalez, B.D.; Bayarri, O.; Acena, B.; Perez, J. Treatment Technologies for Wastewater Reuse: Fate of Contaminants of Emerging Concern. *Adv. Treat. Technol. Urban Wastewater Reuse* **2015**, *20*, 95–100.
4. Patel, M.; Kumar, R.; Kishor, K.; Mlsna, T.; Pittman, C.; Mohan, D. Pharmaceuticals of Emerging Concern in Aquatic Systems: Chemistry, Occurrence, Effects, and Removal Methods. *Chem. Rev.* **2019**, *119*, 3510–3673. [[CrossRef](#)]
5. Zhao, L.; Deng, J.; Sun, P.; Liu, J.; Ji, Y.; Nakada, N.; Qiao, Z.; Tanaka, H.; Yang, Y. Nanomaterials for treating emerging contaminants in water by adsorption and photocatalysis: Systematic review and bibliometric analysis. *Sci. Total Environ.* **2018**, *627*, 1253–1263. [[CrossRef](#)]
6. Kyzas, Z.G.; Fu, J.; Lazaridis, K.N.; Bikiaris, N.D.; Matis, A.K. New approaches on the removal of pharmaceuticals from wastewaters with adsorbent materials. *J. Mol. Liq.* **2015**, *209*, 87–93. [[CrossRef](#)]
7. Gracia-Lor, E.; Sancho, K.V.; Serrano, R.; Hernández, F. Occurrence and removal of pharmaceuticals in wastewater treatment plants at the Spanish Mediterranean area of Valencia. *Chemosphere* **2012**, *87*, 453–462. [[CrossRef](#)]
8. Topkaya, E.; Konyar, M.; Yatmaz, H.C.; Öztürk, K. A comparative study for the degradation of azo dye, pesticide and antibiotic in aqueous solutions. *J. Colloid Interface Sci.* **2014**, *430*, 6–11. [[CrossRef](#)]
9. Stedmon, C.A.; Markager, S.; Bro, R. Tracing dissolved organic matter in aquatic environments using a new approach to fluorescence spectroscopy. *Mar. Chem.* **2003**, *82*, 239–254. [[CrossRef](#)]
10. Stuer-lauridsen, F. Review of passive accumulation devices for monitoring organic micropollutants in the aquatic environment. *Environ. Pollut.* **2005**, *136*, 503–524. [[CrossRef](#)]
11. Liu, X.; Zhang, G.; Liu, Y.; Lu, S.; Qin, P.; Guo, X.; Bi, B.; Wang, L.; Xi, B.; Wu, F.; et al. Occurrence and fate of antibiotics and antibiotic resistance genes in typical urban water of Beijing, China. *Environ. Pollut.* **2019**, *246*, 163–173. [[CrossRef](#)] [[PubMed](#)]
12. Hu, J.; Zhou, J.; Zhou, S.; Wu, P.; Tsang, Y.F. Occurrence and fate of antibiotics in a wastewater treatment plant and their biological effects on receiving waters in Guizhou. *Process Saf. Environ. Prot.* **2018**, *113*, 483–490. [[CrossRef](#)]
13. Luo, Y.; Xu, L.; Rysz, M.; Wang, Y.; Zhang, H.; Alvarez, P.J.J. Occurrence and Transport of Tetracycline, Sulfonamide, Quinolone, and Macrolide Antibiotics in the Haihe River Basin, China. *Environ. Sci. Technol.* **2011**, *45*, 1827–1833. [[CrossRef](#)] [[PubMed](#)]
14. Davies, J.; Davies, D. Origins and Evolution of Antibiotic Resistance. *Microbiol. Mol. Biol. Rev.* **2010**, *74*, 417–433. [[CrossRef](#)] [[PubMed](#)]
15. Carvalho, I.T.; Santos, J.L. Antibiotics in the aquatic environments: A review of the European scenario. *Environ. Int.* **2016**, *94*, 736–757. [[CrossRef](#)] [[PubMed](#)]
16. Di Cesare, A.; Eckert, E.M.; Urso, S.D.; Bertoni, R.; Gillan, D.C.; Wattiez, R.; Corno, G. Co-occurrence of integrase 1, antibiotic and heavy metal resistance genes in municipal wastewater treatment plants. *Water Res.* **2016**, *94*, 208–214. [[CrossRef](#)]
17. Wang, W.L.; Wu, Q.Y.; Huang, N.; Bin Xu, Z.; Lee, M.Y.; Hu, H.Y. Potential risks from UV/H<sub>2</sub>O<sub>2</sub> oxidation and UV photocatalysis: A review of toxic, assimilable, and sensory-unpleasant transformation products. *Water Res.* **2018**, *141*, 109–125. [[CrossRef](#)]
18. Cardinal, P.; Anderson, J.C.; Carlson, J.C.; Low, J.E.; Challis, J.K.; Beattie, S.A.; Bartel, C.N.; Elliott, A.D.; Montero, O.F.; Lokesh, S.; et al. Macrophytes may not contribute significantly to removal of nutrients, pharmaceuticals, and antibiotic resistance in model surface constructed wetlands. *Sci. Total Environ.* **2014**, *482–483*, 294–304. [[CrossRef](#)]
19. Mulla, S.I.; Hu, A.; Sun, Q.; Li, J.; Ashfaq, M.; Yu, C. Biodegradation of sulfamethoxazole in bacteria from three different origins. *J. Environ. Manag.* **2018**, *206*, 93–102. [[CrossRef](#)]

20. Ashfaq, M.; Li, Y.; Wang, Y.; Chen, W.; Wang, H.; Chen, X.; Wu, W.; Huang, Z.; Yu, C.; Sun, Q. Occurrence, fate, and mass balance of different classes of pharmaceuticals and personal care products in an anaerobic-anoxic-oxic wastewater treatment plant in Xiamen, China. *Water Res.* **2017**, *123*, 655–667. [[CrossRef](#)]
21. Homem, V.; Santos, L. Degradation and removal methods of antibiotics from aqueous matrices—A review. *J. Environ. Manag.* **2011**, *92*, 2304–2347. [[CrossRef](#)] [[PubMed](#)]
22. Wang, J.; Wang, S. Removal of pharmaceuticals and personal care products (PPCPs) from wastewater: A review. *J. Environ. Manag.* **2016**, *182*, 620–640. [[CrossRef](#)] [[PubMed](#)]
23. Gonzales, O.; Bayarri, B.; Acena, J.; Perez, S.; Barcelo, D. Treatment Technologies for Wastewater Reuse: Fate of Contaminants of Emerging Concern. *Handb. Environ. Chem.* **2015**, *363*, 5–37.
24. Malesic-Eleftheriadou, N.; Evgenidou, E.; Kyzas, G.Z.; Bikiaris, N.D.; Lambropoulou, D.A. Removal of antibiotics in aqueous media by using new synthesized bio-based poly(ethylene terephthalate)-TiO<sub>2</sub> photocatalysts. *Chemosphere* **2019**, *234*, 746–755. [[CrossRef](#)] [[PubMed](#)]
25. Schaidler, L.A.; Rodgers, K.M.; Rudel, R.A. Review of Organic Wastewater Compound Concentrations and Removal in Onsite Wastewater Treatment Systems. *Environ. Sci. Technol.* **2017**, *51*, 7304–7317. [[CrossRef](#)]
26. Koltsakidou, A.; Antonopoulou, M.; Evgenidou, E.; Konstantinou, I.; Giannakas, A.E.; Papadaki, M.; Bikiaris, N.D.; Lambropoulou, D.A. Photocatalytic removal of fluorouracil using TiO<sub>2</sub>-P25 and N/S doped TiO<sub>2</sub> catalysts: A kinetic and mechanistic study. *Sci. Total Environ.* **2017**, *578*, 257–267. [[CrossRef](#)]
27. Zhang, H.; Zhang, P.; Ji, Y.; Tian, J.; Du, Z. Photocatalytic degradation of four non-steroidal anti-inflammatory drugs in water under visible light by P25-TiO<sub>2</sub>/tetraethyl orthosilicate film and determination via ultra performance liquid chromatography electrospray tandem mass spectrometry. *Chem. Eng. J.* **2015**, *262*, 1108–1115. [[CrossRef](#)]
28. Luiz, D.B.; Jose, H.J.; Moreira, R.F.P.M. A Discussion Paper on Challenges and Proposals for Advanced Treatments for Potabilization of Wastewater in the Food Industry. *Sci. Heal. Soc.* **2012**, *3–24*. [[CrossRef](#)]
29. Fagan, R.; McCormack, D.E.; Dionysiou, D.D.; Pillai, S.C. A review of solar and visible light active TiO<sub>2</sub> photocatalysis for treating bacteria, cyanotoxins and contaminants of emerging concern. *Mater. Sci. Semicond. Process.* **2015**, *42*, 2–14. [[CrossRef](#)]
30. Kang, X.; Liu, S.; Dai, Z.; He, Y.; Song, X.; Tan, Z. Titanium Dioxide: From Engineering to Applications. *Catalysts* **2019**, *9*, 191. [[CrossRef](#)]
31. Qiu, J.; Liu, F.; Yue, C.; Ling, C.; Li, A. A recyclable nanosheet of Mo/N-doped TiO<sub>2</sub> nanorods decorated on carbon nanofibers for organic pollutants degradation under simulated sunlight irradiation. *Chemosphere* **2019**, *215*, 280–293. [[CrossRef](#)] [[PubMed](#)]
32. Thuy-Duong Nguyen-Phan, S.K.; Pham, V.H.; Shin, E.W.; Pham, H.; Jin, S.H.H.; Chung, S.; Kim, E.J. The role of graphene oxide content on the adsorption-enhanced photocatalysis of titanium dioxide/graphene oxide composites. *Chem. Eng. J.* **2011**, *170*, 226–232. [[CrossRef](#)]
33. Shan, A.Y.; Idaty, T.; Ghazi, M.; Rashid, S.A. General Immobilisation of titanium dioxide onto supporting materials in heterogeneous photocatalysis: A review. *Appl. Catal. A Gen.* **2010**, *389*, 1–8. [[CrossRef](#)]
34. Alhaji, M.H.; Khan, K.S.A.; Muhammad, A.H.A. Recent developments in immobilizing titanium dioxide on supports for degradation of organic pollutants in wastewater—A review. *Int. J. Environ. Sci. Technol.* **2017**, *14*, 2039–2052. [[CrossRef](#)]
35. Xing, Z.; Li, J.; Wang, Q.; Zhou, W.; Tian, G.; Pan, K.; Tian, C.; Zou, J.; Fu, H. A Floating Porous Crystalline TiO<sub>2</sub> Ceramic with Enhanced Photocatalytic Performance for Wastewater Decontamination. *Eur. J. Inorg. Chem.* **2013**, *2013*, 2411–2417. [[CrossRef](#)]
36. Buzarovska, A.; Gualandi, C.; Parrilli, A.; Scandola, M. Effect of TiO<sub>2</sub> nanoparticle loading on Poly(L-lactic acid) porous scaffolds fabricated by TIPS. *Compos. Part B Eng.* **2015**, *81*, 189–195. [[CrossRef](#)]
37. Athanasoulia, I.; Mikropoulou, M.; Karapati, S. Study of thermomechanical and antibacterial properties of TiO<sub>2</sub>/Poly(lactic acid) nanocomposites. *Mater. Today Proc.* **2018**, *5*, 27553–27562. [[CrossRef](#)]
38. Rezwani, K.; Chen, Q.Z.; Blaker, J.J.; Roberto, A. Biodegradable and bioactive porous polymer/inorganic composite scaffolds for bone tissue engineering. *Biomaterials* **2006**, *27*, 3413–3431. [[CrossRef](#)]
39. Shaikh, K.H.; Rathore, T.; Kaur, H. Poly(Lactic Acid) Grafting of TiO<sub>2</sub> Nanoparticles: A Shift in Dye Degradation Performance of TiO<sub>2</sub> from UV to Solar Light. *Chem. Sel.* **2017**, *2*, 6901–6908.

40. Zhu, Y.; Buonocore, G.G.; Lavorgna, M. Photocatalytic Activity of PLA/TiO<sub>2</sub> Nanocomposites and TiO<sub>2</sub>-active Multilayered Hybrid Coatings. *Ital. J. Food Sci.* **2012**, *24*, 102–107.
41. Zhu, Y.; Buonocore, G.G.; Lavorgna, M.; Ambrosio, L. Poly(lactic acid)/Titanium Dioxide Nanocomposite Films: Influence of Processing Procedure on Dispersion of Titanium Dioxide and Photocatalytic Activity. *Polym. Compos.* **2011**, *32*, 519–528. [[CrossRef](#)]
42. Hou, X.; Yibing, C.; Muhammad, M.; Xiaofei, S.; Qiang, Y.; Fenglin, H.; Qufu, W. Deposition of TiO<sub>2</sub> Nanoparticles on Porous Polylactic Acid Fibrous Substrates and Its Photocatalytic Capability. *J. Nanomed. Nanotechnol.* **2018**, *18*, 5617–5623. [[CrossRef](#)] [[PubMed](#)]
43. Kaseem, Z.U.; Hamad, M.; Rehman, K. Review of Recent Advances in Polylactic. *Mater. Sci. Eng. C* **2019**, *12*, 3659.
44. Carpenter, D.O.; Arcaro, K.; Spink, D.C. Understanding the Human Health Effects of Chemical Mixtures. *Environ. Health Perspect.* **2002**, *110*, 25–42. [[CrossRef](#)] [[PubMed](#)]
45. Stergiou, D.V.; Diamanti, K.; Gournis, D.; Prodromidis, M.I. Comparative study of different types of graphenes as electrocatalysts for ascorbic acid. *Electrochem. Commun.* **2010**, *12*, 1307–1309. [[CrossRef](#)]
46. Yang, Z.; Peng, H.; Wang, W.; Liu, T. Crystallization behavior of poly( $\epsilon$ -caprolactone)/layered double hydroxide nanocomposites. *J. Appl. Polym. Sci.* **2010**, *116*, 2658–2667. [[CrossRef](#)]
47. Papageorgiou, G.Z.; Terzopoulou, Z.; Bikiaris, N.D.; Triantafyllidis, K.S.; Diamanti, E.; Gournis, D.; Klonos, P.; Giannoulidis, E.; Pissis, P. Evaluation of the formed interface in biodegradable poly(l-lactic acid)/graphene oxide nanocomposites and the effect of nanofillers on mechanical and thermal properties. *Thermochim. Acta* **2014**, *597*, 48–57. [[CrossRef](#)]
48. Nerantzaki, M.; Prokopiou, L.; Bikiaris, N.D.; Patsiaoura, D.; Chrissafis, K.; Klonos, P.; Kyritsis, A.; Pissis, P. In situ prepared poly(DL-lactic acid)/silica nanocomposites: Study of molecular composition, thermal stability, glass transition and molecular dynamics. *Thermochim. Acta* **2018**, *669*, 16–29. [[CrossRef](#)]
49. Bet-Moushoul, E.; Mansourpanah, Y.; Farhadi, K.; Tabatabaei, M. TiO<sub>2</sub> nanocomposite based polymeric membranes: A review on performance improvement for various applications in chemical engineering processes. *Chem. Eng. J.* **2016**, *283*, 29–46. [[CrossRef](#)]
50. Klonos, P.; Kriptou, S.; Kyritsis, A.; Papageorgiou, G.Z.; Bikiaris, N.D.; Gournis, D. Glass transition and segmental dynamics in poly(l-lactic acid)/graphene oxide nanocomposites. *Thermochim. Acta* **2015**, *617*, 44–53. [[CrossRef](#)]
51. Bourlinos, A.B.; Gournis, D.; Petridis, D.; Szabó, T.; Szeri, A.; Dékány, I. Graphite oxide: Chemical reduction to graphite and surface modification with primary aliphatic amines and amino acids. *Langmuir* **2003**, *19*, 6050–6055. [[CrossRef](#)]
52. Klonos, P.; Terzopoulou, Z.; Koutsoumpis, S.; Zidropoulos, S.; Kriptou, S.; Papageorgiou, G.Z.; Bikiaris, D.N.; Kyritsis, A.; Pissis, P. Rigid amorphous fraction and segmental dynamics in nanocomposites based on poly(L-lactic acid) and nano-inclusions of 1–3D geometry studied by thermal and dielectric techniques. *Eur. Polym. J.* **2016**, *82*, 16–34. [[CrossRef](#)]
53. Terzopoulou, Z.; Klonos, P.A.; Kyritsis, A.; Tziolas, A.; Avgeropoulos, A.; Papageorgiou, G.Z.; Bikiaris, D.N. Interfacial interactions, crystallization and molecular mobility in nanocomposites of Poly(lactic acid) filled with new hybrid inclusions based on graphene oxide and silica nanoparticles. *Polymer* **2019**, *166*, 1–12. [[CrossRef](#)]
54. Papageorgiou, G.Z.; Achilias, D.S.; Nanaki, S.; Beslikas, T.; Bikiaris, N.D. PLA nanocomposites: Effect of filler type on non-isothermal crystallization. *Thermochim. Acta* **2010**, *511*, 129–139. [[CrossRef](#)]
55. Babić, S.; Periša, M.; Škorić, I. Photolytic degradation of norfloxacin, enrofloxacin and ciprofloxacin in various aqueous media. *Chemosphere* **2013**, *91*, 1635–1642. [[CrossRef](#)]
56. Konstantinou, I.K.; Albanis, T.A. TiO<sub>2</sub>-assisted photocatalytic degradation of azo dyes in aqueous solution: Kinetic and mechanistic investigations: A review. *Appl. Catal. B Environ.* **2004**, *49*, 1–14. [[CrossRef](#)]
57. Hir, Z.A.M.; Moradihamedani, P.; Abdullah, A.H.; Mohamed, M.A. Immobilization of TiO<sub>2</sub> into polyethersulfone matrix as hybrid film photocatalyst for effective degradation of methyl orange dye. *Mater. Sci. Semicond. Process.* **2017**, *57*, 157–165. [[CrossRef](#)]
58. Tahir, C.; Qazi, I.A.; Anwar, M.; Arshad, M.; Quddos, A. Enhanced photodegradation of titania loaded polyethylene films in a humid environment. *Int. Biodeterior. Biodegrad.* **2016**, *113*, 287–296.

59. Agüera, A.; Perez Estrada, L.A.; Ferrer, I.; Thurman, E.M.; Malato, S.; Fernandez-Alba, A.R. Application of time-of-flight mass spectrometry to the analysis of phototransformation products of diclofenac in water under natural sunlight. *J. Mass Spectrom.* **2005**, *40*, 908–915. [[CrossRef](#)]
60. Koltsakidou, A.; Antonopoulou, M.; Evgenidou, E.; Konstantinou, I. A comparative study on the photo-catalytic degradation of Cytarabine anticancer drug under  $\text{Fe}^{3+}/\text{H}_2\text{O}_2$ ,  $\text{Fe}^{3+}/\text{S}_2\text{O}_8^{2-}$ , and  $[\text{Fe}(\text{C}_2\text{O}_4)_3]^{3-}/\text{H}_2\text{O}_2$  processes. Kinetics, identification, and in silico toxicity assessment of generated transformation products. *Environ. Sci. Pollut. Res.* **2019**, *26*, 7772–7784. [[CrossRef](#)]



© 2020 by the authors. Licensee MDPI, Basel, Switzerland. This article is an open access article distributed under the terms and conditions of the Creative Commons Attribution (CC BY) license (<http://creativecommons.org/licenses/by/4.0/>).